Made available through Montana State University's ScholarWorks

Deep Learning Predictions of SST at the Atlantis II Seamounts with Links to Global Teleconnections

Kerstin E. Cullen; Carolyn A. Reynolds; Adam Rydbeck

Accessibility Disclaimer:

For a more accessible version of this document, please submit an accessibility request form through the Montana State University Library website.

Deep Learning Predictions of SST at the Atlantis II Seamounts with Links to Global Teleconnections

KERSTIN E. CULLEN,[a] CAROLYN A. REYNOLDS,[b] AND ADAM RYDBECK[c]

[a] *Montana State University, Bozeman, Montana*
[b] *Atmospheric Science Division, U.S. Naval Research Laboratory, Monterey, California*
[c] *U.S. Naval Research Laboratory Stennis, Hancock County, Mississippi*

(Manuscript received 1 August 2024, in final form 31 January 2025, accepted 14 February 2025)

ABSTRACT: Located in the western North Atlantic, the subsurface temperature and salinity structure at the Atlantis II Seamounts is sensitive to fluctuations in the Gulf Stream, and historical ocean structure profiles at this location show a bimodal distribution, making seasonal climatologies a poor predictor of ocean states. Historical CMIP6 ensemble means show dynamic changes in temperature between 1980 and 2007 (0.5°C), with no corresponding change in sea surface height anomalies, suggestive of decadal changes independent of the Gulf Stream position. While previous deep learning models have been able to predict SST globally, the Gulf Stream region has some of the lowest accuracy and shortest forecast horizons. We use a deep learning (convolutional neural network) model to predict sea surface height anomalies and sea surface temperature for 1 month to 2 years, focusing on the Atlantis II Seamounts. The training dataset consists of the global 1850–2007 CMIP6 temperature, height, and mixed layer depth that capture climate modes of variability that impact the Gulf Stream. We test our model predictions with Ocean Reanalysis System 5 (ORAS5) reanalysis data. Our model can beat the climatology for up to 24 months by predicting different decadal regimes in the Gulf Stream. Using back-propagation saliency maps, we connect Atlantis II Seamounts predictions to multiple global modes of climate variability, such as the North Atlantic Oscillation, the Indian Ocean dipole, the Pacific decadal oscillation, and ENSO.

KEYWORDS: Boundary currents; North Atlantic Oscillation; Sea surface temperature; Seasonal forecasting; Deep learning

1. Introduction

The Atlantis II Seamounts are located in the North Atlantic (38.40°N, 62.84°W, Fig. 1), in a region of interest due to the dynamic ocean states and the challenge in describing acoustic profiles. Ocean states at this location are sensitive to fluctuations, meanders, and loops of the Gulf Stream (Taylor and Stephens 1998) and thus have strong connections to basin-scale changes in forcing (i.e., climate modes of variability) that impact the Gulf Stream (Chaudhuri et al. 2011). In addition, the topography of the seamounts impacts Gulf Stream meanders (and thus local density profiles) by vertically deflecting isopycnals and perturbing eddies (Vastano and Warren 1976). Historical subsurface density profiles at the North Atlantis II Seamounts show a bimodal distribution (Walters et al. 2024), reflecting the location of the Gulf Stream relative to the Atlantis II Seamounts and the corresponding warm/cold ocean state regime (Gispen and Schmeits 2001; Bane and Dewar 1988).

As the accuracy of long-term forecasts (>6 months) using dynamical ocean models decreases with time (Lu et al. 2020), monthly climatologies are still used for forecast horizons from 6 months to 2 years in many practical applications (Carnes 2009). However, due to the bimodal distribution driven by changes in the position of the Gulf Stream, the climatological mean does not reflect any state occurring at the Atlantis II Seamounts (Walters et al. 2024). Furthermore, climate change reduces the skill of long-term forecasts based on the climatological mean. Linear regressions and stochastic predictive models do not account for complex nonlinear feedbacks that control ocean states, such as Gulf Stream meander formation (Pratt et al. 1991) and Gulf Stream temperature front/North Atlantic Oscillation interaction (Paolini et al. 2024). Due to this region's complex interactions with global atmospheric forcing, large-scale patterns in the Gulf Stream, and local topography, the Atlantis II Seamounts are an excellent candidate to test if deep learning models can forecast sea surface temperature (SST) in a changing climate.

a. Forcing in the Gulf Stream

The position, structure, and total transport of the Gulf Stream vary on subseasonal and greater time scales (McCarthy et al. 2012; Sato and Rossby 1995) and are coupled with both atmospheric (Joyce et al. 2009) and oceanic forcing (Sanchez-Franks and Zhang 2015). Wind variability influences the meridional position of the Gulf Stream (by altering the position of latitudinal neutral wind stress curl) and the formation of mesoscale Gulf Stream features (Guo et al. 2023), both of which affect ocean states at the Atlantis II Seamounts (Sanchez-Franks et al. 2016). Rossby waves generated from remote wind conditions impact Gulf Stream variability at the Atlantis II Seamounts with predictability between 1 and 24 months (Taylor and Stephens 1998; Watelet et al. 2017). Buoyancy changes within the North Atlantic, such as the Atlantic meridional overturning circulation, force the position of the

Corresponding author: Kerstin Cullen, kerstin.cullen@gmail.com

DOI: 10.1175/JPO-D-24-0099.1

For information regarding reuse of this content and general copyright information, consult the AMS Copyright Policy (www.ametsoc.org/PUBSReuseLicenses).

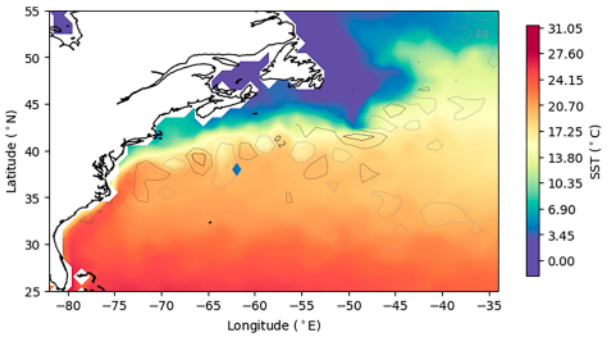


FIG. 1. Map of ORAS5 SST (shaded) for January 2023 over the Gulf Stream, showing the Atlantis Seamounts II (diamond). Light gray contours indicate the negative 0.02-m contours, and black indicates the positive 0.02-m contours for sea surface height anomalies.

Gulf Stream on interannual time scales (Joyce and Zhang 2010; Hameed et al. 2018).

Global modes of climate variability associated with perturbations in the Gulf Stream include the Atlantic meridional mode (Hameed et al. 2018; Wolfe et al. 2019) and the Atlantic multidecadal oscillation (Nigam et al. 2018). Of particular relevance is the North Atlantic Oscillation (NAO), the primary mode of atmospheric wind variability over the Atlantic and a well-documented driver of the variability of the Gulf Stream (Barnston and Livezey 1987; Bader and Latif 2005; Paolini et al. 2024). The NAO forces the Gulf Stream by latitudinally shifting wind patterns and generating westward-propagating oceanic Rossby waves (Gangopadhyay et al. 2016). Variability in the Gulf Stream linked to the NAO includes increased the northward position and Ekman transport during the positive phase of the NAO (Taylor et al. 1998; Visbeck et al. 2003), from a 1-month to 3-yr lag in ocean response (Frankignoul et al. 2001; Taylor and Gangopadhyay 2001; Paolini et al. 2024). Other modes of variability with links to the Gulf Stream include the Indian Ocean dipole (IOD), which affects interannual predictability in the Eastern Hemisphere (Webster et al. 1999), and El Niño–Southern Oscillation (ENSO), which influences predictability in the Pacific and globally (Bjerknes 1969). The position of the Gulf Stream shifts with ENSO events (Taylor et al. 1998; Sanchez-Franks et al. 2016; Seidov et al. 2019), through nonlinear ocean/atmospheric interaction changing wind patterns (Jiménez-Esteve and Domeisen 2020), with Gulf Stream response lagging up to 1 year (Taylor et al. 1998). Fluctuations in the Gulf Stream are synchronized with the fluctuations in the Pacific's western boundary current (the Kuroshio) on decadal time scales due to global changes in wind patterns (Kohyama et al. 2021).

In addition, this region is experiencing a substantial increase in temperature and heat content with climate change (Saba et al. 2016; Yamagami et al. 2022), which adds to variability in strength and position (Dong et al. 2019). Decadal variability within the North Atlantic is large compared to observed trends associated with climate change, and trends are challenging to resolve with satellite data (Chi et al. 2021). In 2008, the Gulf Stream shifted northward into a new spatial distribution measured with sea surface height (SSH) and SST and has maintained this unprecedented pattern (Gonçalves Neto et al. 2021). Models predict a slowing Gulf Stream velocity (Hu and Bates 2018), a northward shift in the north wall position (Hand et al. 2019), and suggest an increase in heat may also broaden Gulf Stream meanders, decreasing the SSH amplitude of these features (Yun et al. 2024). Multiple studies use in situ data to quantify warming within the Gulf Stream (Yang et al. 2016; Caesar et al. 2018; Smeed et al. 2018). Todd and Ren (2023) showed that increased heat within the Gulf Stream system is associated with increased stratification and zonal broadening; this increase in heat may slow down horizontal transport within the current system (Dong et al. 2019).

b. *AI ocean and atmosphere prediction modeling efforts*

Deep learning and neural network predictive models are increasingly used in ocean and atmospheric science (Ardabili et al. 2019; Airlangga 2024; Ali et al. 2021; Hamdan et al. 2024; Jeon and Kim 2024; Wang et al. 2023), with particular success at the subseasonal to seasonal range (2 weeks–2 years), relative to dynamic models (Barnes et al. 2023; van Straaten et al. 2023; Airlangga 2024). Of particular interest is the success of modeling efforts in predicting the climate modes of variability due to their links to predicting SST (Cullen et al. 2022; Wei et al. 2024). Multiple neural network models have made multiseason predictions using climate model simulations and reanalysis of the Indian Ocean dipole (Ratnam et al. 2020; J. Liu et al. 2021; Sarkar et al. 2021; Ling et al. 2022; Janmaijaya et al. 2024), ENSO (Ham et al. 2019; He et al. 2019; Geng and Wang 2021; Mu et al. 2021; Gao et al. 2023; Rivera Tello et al. 2023; Zhou and Zhang 2024; Wang and Huang 2024), NAO (Yuan et al. 2019; Mu et al. 2020; Luo et al. 2021; Mu et al. 2023), the Atlantic and Benguela Niño (Bachelery et al. 2024), and Atlantic multidecadal oscillation (G. Liu et al. 2021). To date, the most successful ocean and atmospheric artificial intelligence (AI) predictive models are not fully coupled (Wang et al. 2023; Lam et al. 2022; Kim et al. 2023; Mu et al. 2021, 2023).

Multiple efforts used neural networks to predict ocean temperature at various scales and geographical locations, many using only SST data as the predictor (Xie et al. 2020; Xiao et al. 2019; Yu et al. 2020; Sarkar et al. 2020; Choi et al. 2023; Krestenitis et al. 2024). Global SST predictions made by modeling efforts of Wei et al. (2024) and Xu et al. (2023) were successful on short (less than 6 months) time scales. Both Xie et al. (2024) and Liu et al. (2024) used their deep learning models to predict three-dimensional ocean temperature for up to 2 months at high resolution in constrained locations, using multiple ocean and atmospheric variables as predictands. While restricted to coastal SST, Kim et al. (2023) used a graphical neural network to make forecasts at a range of time scales, and Snoussi et al. (2024) used deep learning to forecast upwelling. Using SST and atmospheric variables, Taylor and Feng (2022) made global SST predictions for up to 2 years, with most regions exhibiting skillful predictions for up to 1 year.

However, predictions in the Gulf Stream region and other western boundary currents were successful for up to 6 months (Taylor and Feng 2022).

Due to the phase 6 of the Coupled Model Intercomparison Project' (CMIP6) length as a time series and robust performance relative to reanalysis data (Cheng and Zhu 2016; Tang and Duan 2021), multiple modeling efforts used CMIP6 data and reanalysis to train neural networks (Qi et al. 2023; Su et al. 2024). Of particular interest are efforts that used ocean data to make subseasonal to seasonal predictions, such as Pan et al. (2022) who used subsurface ocean data from 30 CMIP5 and CMIP6 models to train a convolutional neural network (CNN), and then tested with reanalysis data. CMIP6 data have been beneficial for training CNNs to predict ENSO (Ham et al. 2019; Zhou and Zhang 2024; Wang and Huang 2024; Lops et al. 2023) and IOD (Feng et al. 2022) as CMIP models simulate this phenomenon well (Bellenger et al. 2014). However, other studies such as Bachelery et al. (2024) found that CMIP6 data are not a suitable training dataset due to the poor way CMIP6 resolves the Atlantic Niño. To our knowledge, no studies have tested the suitability of CMIP6 models for training CNN for Gulf Stream prediction.

We aim to build a deep learning (CNN) long-term prediction model that is more skilled than the seasonal cycle at predicting SST at the Atlantis II Seamounts. To do this, we explore the following questions:

1) Is CMIP6 a suitable training/validation dataset for the CNN model for the Gulf Stream, and how does it compare to Ocean Reanalysis System 5 (ORAS5) data?
2) Can the CNN model make long-term (2-yr) SST predictions that improve over the seasonal cycle?
3) What global teleconnections impact SST at the Atlantis II Seamounts in the model, and can we visualize them using modern interpretation techniques?

While many modeling efforts forecast global ocean surface variables, these global efforts often show poorer forecasts for the Gulf Stream region (Taylor and Feng 2022). In contrast to these previous efforts, we constrained our model output to the North Atlantis Seamounts to optimize the tuning of hyperparameters, as the physics of the Gulf Stream and western boundary currents are unique in the global ocean. In addition, by limiting our model to the Atlantis II Seamounts, we aim to maximize the interpretability of the forcing and global teleconnections SST at the Atlantis II Seamounts.

2. Methods

Our predictor data consisted of global maps of SST, SSH anomalies (SSHAs), and mixed layer depth (MLD). We used model output and reanalysis datasets to maximize our time series of available data. The model output consisted of the ensemble mean of 26 historical CMIP6 ensemble members, with ocean resolutions varying from 0.1° to 1°. We used CMIP6 models as the time series is sufficiently large (1850–2007) to resolve 2-yr predictions (Ham et al. 2019), while the ensemble mean is more accurate than any individual member for global and Gulf Stream SST (Borchert et al. 2021; Scafetta 2023; Dorrington et al. 2021). Note the limitations of CMIP6 ensemble means include a bias in the spatial distribution of SSHAs during ENSO (Sardana et al. 2024) and potential to smooth Gulf Stream meanders (Dorrington et al. 2021). While we acknowledge the Gulf Stream is a coupled ocean/atmosphere problem, we only used ocean data as there are inconsistencies with ocean and atmospheric variables in CMIP6 [e.g., models with most accurate SST tend to have the least accurate winds (Richter and Tokinaga 2020)], and Mu et al. (2021) caution against inputting ocean/atmospheric together into a CNN due to the difference in physics between these two systems. Our testing data consist of ORAS5 reanalysis data from 1951 to 2023 for mixed layer depth, sea surface temperature, and sea surface height anomalies. We derived SSHAs from sea surface height, with the yearly climatology subtracted. We remapped all data to a 1° grid projection, deseasonalized, and normalized into anomalies (SSTa, SSHa, MLDa) based on the overlap period between the two datasets. The anomalies a are

$$a = \frac{X - \mu}{\sigma}, \tag{1}$$

where X is the variable's value, μ is the temporal mean, and σ is the temporal variance (the ranges of variance we used to normalize each pixel are found in Fig. 4). We applied exponential smoothing (i.e., only uses information from previous time steps) to the predictand (Atlantis II Seamount time series) data for all validation/training/testing.

We split the data into 15% validation (CMIP6, 1850–1873), 70% training (CMIP6, 1874–1997), and 15% testing (ORAS5, 1998–2020). We selected the validation period so that the variability of that time series was within the variability of the training dataset, as demonstrated by Hamid et al. (2021).

Model and analysis

To forecast SSTa at the Atlantis Seamounts II (i.e., a single point at 38°N, 62°E), we used a convolutional neural net. Input (predictor) data consisted of normalized SST, SSH, and MLD anomalies fields for the seven previous months. The architecture of the deep learning model consisted of three convolutional layers with ReLU activation,[1] with max pooling and batch normalization between each layer (Fig. 2). The final steps consist of two hidden layers with ReLU activation (Fig. 2). Output (predictand) consisted of SSTa from 1 to 24 months. As current dynamical models reliably forecast ocean states at 0–6-month range (Weisheimer et al. 2009), we optimized hyperparameters (tuning) for 12-month predictions. We used a batch size of 70 (the batch size is the number of data points used before updating the model) and 63 epochs (the number of times the CNN model runs through the complete dataset during training).

[1] That is, rectified linear activation function, or rectified linear unit, commonly used in deep learning models as noted by Glorot et al. (2011) due to ReLU's performance.

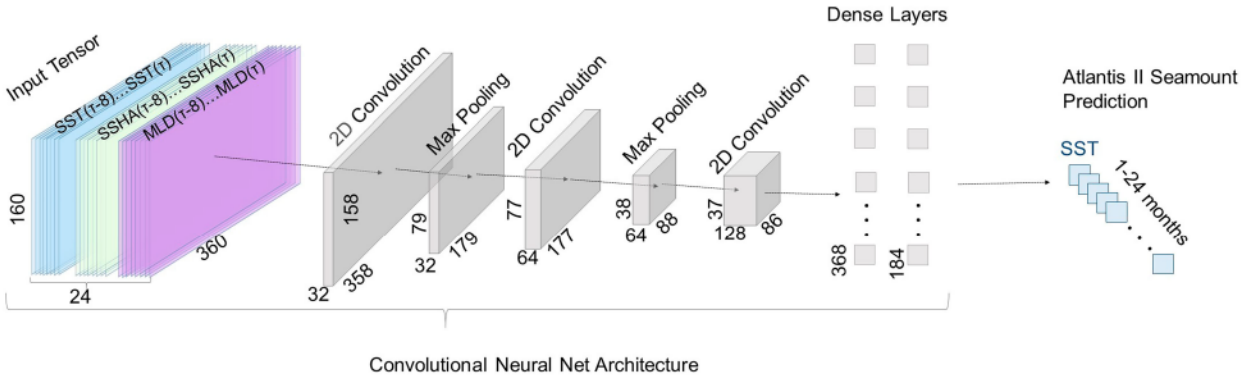


FIG. 2. Architecture of the deep learning model. Input data consist of normalized global maps of SST, SSHAs, and MLD for the eight preceding months. This input tensor is put through three convolutional layers using ReLU activation (32, 64, and 128 filters, respectively). Between each convolutional layer, we use batch normalization and a max pooling layer. Output is SST anomalies from 1 month to 2 years.

Using these hyperparameters, we tested 12 random seeds and selected the model that performed best for further analysis. We note that in the ensemble of 12 models trained with the same hyperparameters but varying the random seed, the models disperse more (ensemble variance is between 0.75 and 1.5) when predictand testing data are outside the bounds of (e.g., warmer than) the training dataset, with only 30% of the models capturing this increase in temperature. In contrast, when the predictand testing data are within the bounds of the training data, the ensemble variance was less than 0.5. This dispersion during the warm period was fairly consistent for models with hyperparameters that were able to beat the seasonal cycle. We used this ensemble spread to inform both our hyperparameter selection and individual model selection where the testing dataset is outside the bounds of the training dataset.

To evaluate the 1-day prediction for the Atlantis II Seamounts, we used mean absolute percent error (MAPE), root-mean-square error (RMSE), and absolute error ($|E|$) as used by Yu et al. (2020), where

$$\mathrm{MAPE} = \frac{100}{n}\sum_{i=1}^{n}\left|\frac{X_i^{\mathrm{pre}} - X_i^{\mathrm{obs}}}{X_i^{\mathrm{pre}}}\right|, \tag{2}$$

$$\mathrm{RMSE} = \sqrt{\sum_{i=1}^{n}\frac{(X_i^{\mathrm{pre}} - X_i^{\mathrm{obs}})^2}{n}}, \tag{3}$$

$$|E| = |X_i^{\mathrm{pre}} - X_i^{\mathrm{obs}}|, \tag{4}$$

where X_i^{obs} is the value of the observation at time i, X_i^{pre} is the predictive value at time i, and n is the number of steps in the time series.

We created relevancy back-propagation saliency maps using the method of Rebuffi et al. (2020) to quantify model behavior and isolate physical phenomena that impact the Atlantis II Seamounts. This interpretation method quantifies how each neuron (displayed as a spatial map) contributes to predictions and performs well on Bommer et al.'s (2024) test (relative to other interpretability methods) for robustness and complexity. To disentangle the sign of relevance (Mamalakis et al. 2022) and make climate modes of variability visible to the human eye in the saliency maps, we only used positive α relevancy (Bommer et al. 2024).

3. Variability in datasets for the CNN model

a. *Variability at the Atlantis II Seamounts within CMIP6 ensemble*

At the Atlantis II Seamounts, the first quartile of deseasonalized CMIP6 ensemble members varies between 0.27° and 1.19°C for SST (Fig. 3a), between 0.076 and 0.038 m for SSHAs (Fig. 3b), and between 115 and 12 m for MLD (Fig. 3c). In comparison, the variability of the CMIP6 ensemble mean ranges from −0.61° to 0.83°C in SST, from −0.061 to 0.042 m for SSHAs, and from −69 to 58 m for MLD (Figs. 3a–c).

In SSHAs, most variability occurs in decadal scales (Fig. 3b), most likely associated with decadal changes in the NAO and Atlantic multidecadal oscillation (Paolini et al. 2024). To a lesser extent, SST exhibits some of these decadal signals, such as between 1940 and 1990 (Fig. 3b). The most considerable variability in MLD exists on subseasonal (monthly) time scales (Fig. 3c). SST at the Atlantis II Seamounts exhibits a robust increasing trend between 1980 and 2007 of 0.83°C (Fig. 3a). No trend is visible in SSHAs during that period, but a slight (0.023 m) occurs over the entire 157-yr time span (Fig. 3b). The warming trend in SST and the associated new ocean states that were not seen previously in the time series will be a challenge in making deep learning forecasts.

b. *Comparison of predictors*

PREDICTOR DATASETS

To compare the variability of training/validation datasets (CMIP6 ensemble mean) and the testing dataset (ORAS5), we present the standard deviations of global maps of these

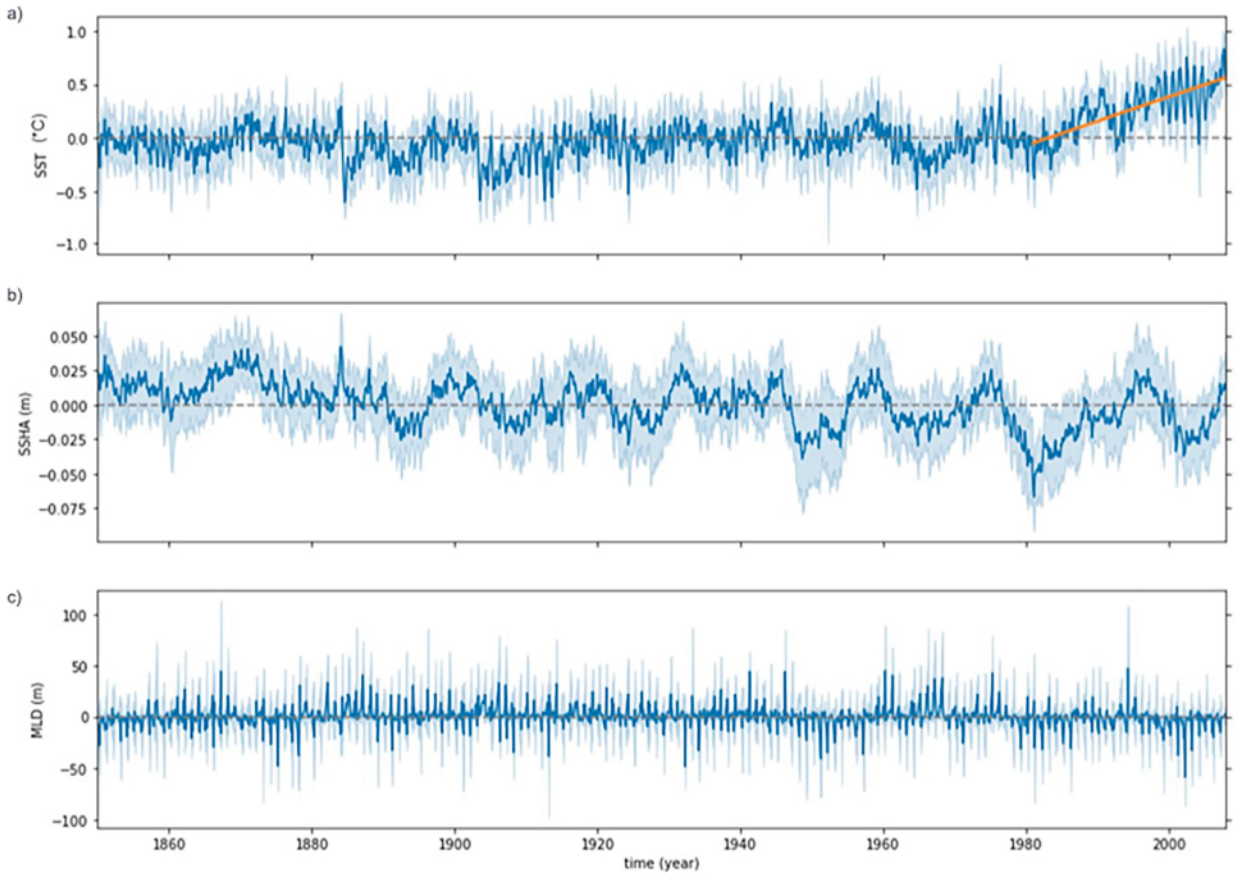


FIG. 3. Time series of CMIP6 data (seasonal cycle removed) at the Atlantis II Seamounts (38°N, 62°E), with ensemble mean (bold), and ensemble standard deviation (shaded) for (a) SST, (b) SSHAs, and (c) MLD. The orange line indicates the recent trend in temperature.

datasets (not normalized). The standard deviation of SST in the global input datasets is most minor (<1°C) in the equatorial Indian Ocean and western Pacific in both CMIP6 ensemble mean and ORAS5 reanalysis (Figs. 4a,b). While the most substantial SST variability occurs in the regions of western boundary currents such as the Kuroshio in the Pacific and the Gulf Stream, the maximum variability in the Gulf Stream is higher in ORAS5 (9.5°C) than in the CMIP6 ensemble mean (8.6°C, Figs. 4a,b).

The minimum standard deviation in SSHAs is 0.004 m in the CMIP6 ensemble mean but 0.018 m in ORAS5 (Figs. 4c,d). Globally, SSHA variability is much more considerable in ORAS5, with the maximum occurring in the Gulf Stream (0.33 m), relative to CMIP6 ensemble mean of 0.184 m (Figs. 4c,d). SSH also has substantial variability in ORAS5 in the Southern Ocean (maximum 0.31 m) that is absent (i.e., between 0.05 and 0.01) in the CMIP6 ensemble mean (Figs. 4c,d). Beyond the Southern Ocean, the global pattern of SSHA variability in the CMIP6 ensemble mean broadly matches that of ORAS5, if not the magnitude (Figs. 4c,d).

In MLD, variability is minimum near zero at low latitudes (30°S–30°N) in both datasets (Figs. 4e,f). The maximum standard deviation in CMIP6 is 422 m, higher than that of ORAS5 at 331 (Figs. 4e,f). The greatest MLD variability (outside of high latitudes and in the Southern Ocean) occurs within the Gulf Stream (Figs. 4e,f). The maximum values in CMIP6 and ORAS5 are 102 and 64 m, respectively. In contrast to SST and SSHAs, variability is higher in the CMIP6 ensemble mean for MLD than in ORAS5.

As the two datasets (i.e., CMIP6 ensemble mean and ORAS5) occur during different periods, we expect variability to be different. For example, as the CMIP6 dataset is an ensemble mean, we expect it to be smoother, even if individual members may exhibit more substantial spatial variability, where ORAS5 may partially resolve eddies (if they are large enough), while the CMIP6 ensemble mean does not (Figs. 4c,d). The success of the deep learning model will depend on the convolutions being able to filter out smaller-scale noise in SSH. Less variability in mixed layer depth exists in ORAS5 relative to CMIP6 at deep-water formation sites (Figs. 4c,d). CMIP6 model iterations show deep-water formation slowing in the later quarter of this time series (Hameed et al. 2018; Chen et al. 2023), where CMIP6 overlaps with ORAS5. As the ORAS5 time series occurs during a period of weakened deep-water formation relative to the full CMIP6 dataset, the standard deviations may reflect this.

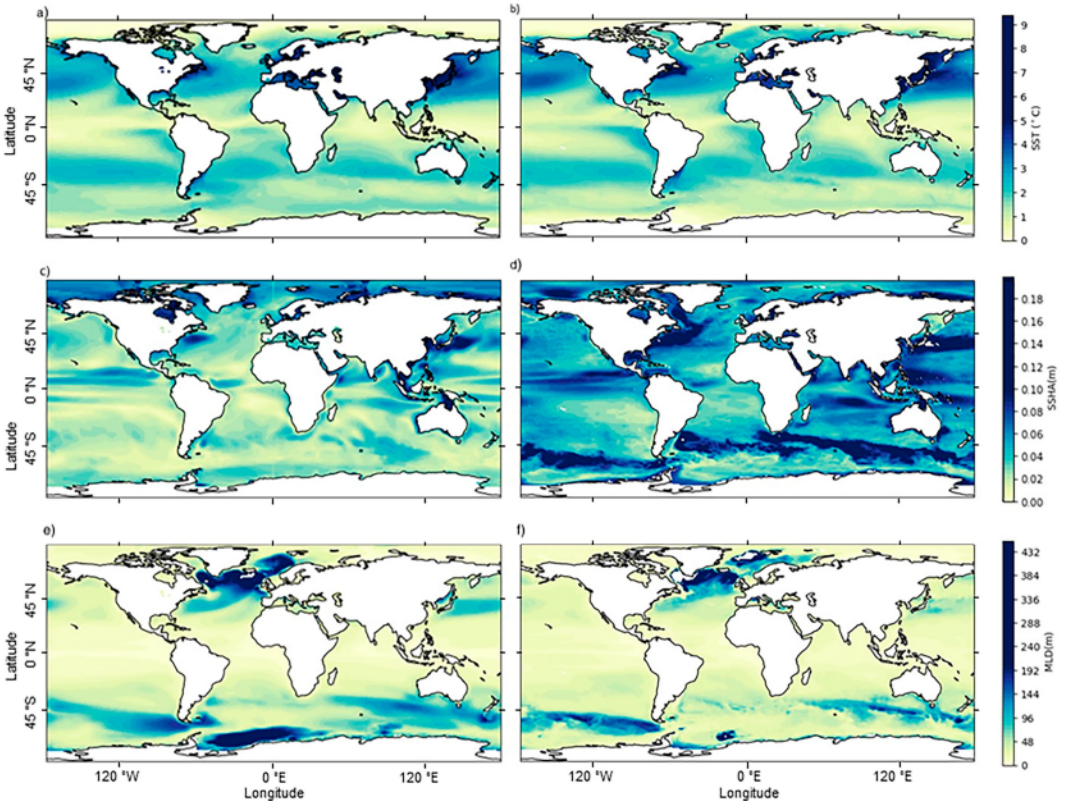


FIG. 4. (left) Standard deviation maps of CMIP6 ensemble mean and (right) ORAS5 reanalysis gridded to 1° resolution for (a),(b) SST, (c),(d) SSHAs, and (e),(f) MLD.

c. *Predictand datasets*

As the CMIP6 ensemble mean and ORAS5 overlap between 1958 and 2007 (Figs. 5a,b), we can contrast the predictand datasets (i.e., normalized anomalies with exponential smoothing). In SST, ORAS5 varies from −1.71 to 1.18 (unitless), while CMIP6 varies from −1.73 to 2.40 (Fig. 5a). While both datasets show rapid warming at the Atlantis II Seamounts, there is displacement when this occurs: In CMIP6, this rapid warming occurs between 2004 and 2007, but in ORAS, this does not occur until 2015–18 (Fig. 5a).

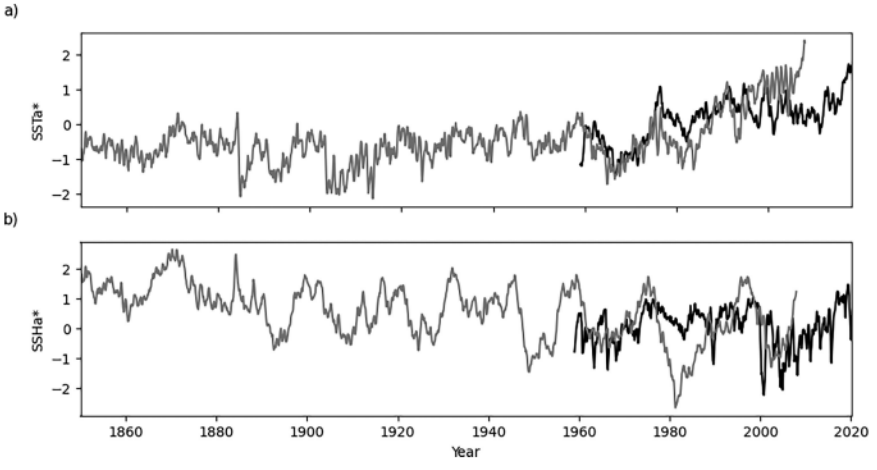


FIG. 5. Time series of the CMIP6 ensemble mean (gray), and ORAS5 (black) deseasonalized normalized anomalies (unitless), smoothed with prior facing exponential smoothing (smoothing factor = 0.1) for (a) SSTa and (b) SSHa.

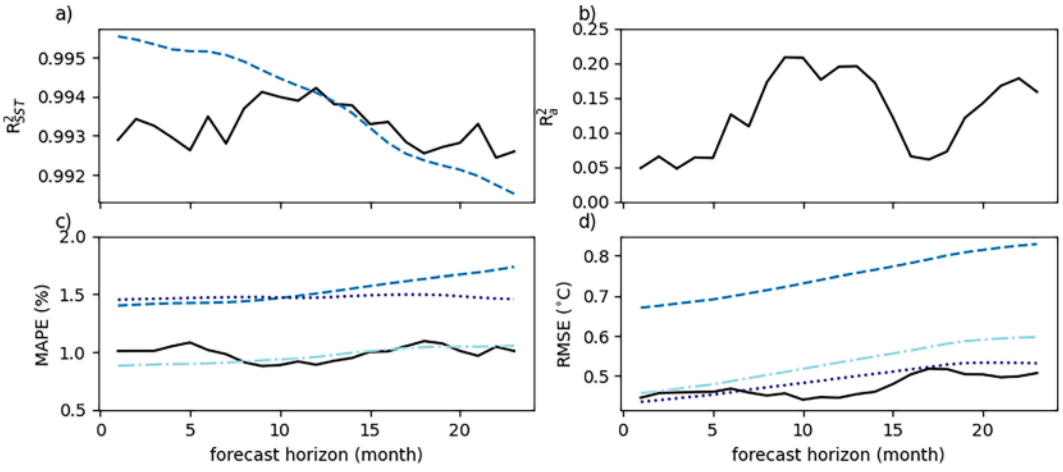


FIG. 6. Evaluation of SST predictions for 1–24-month forecast horizon. Black line indicates the deep learning model predictions SST_{CNN}, and light blue dashed line indicates the evaluation of the (1958–2007) seasonal cycle (SST_{full}) as a comparison for (a) R^2 of SST (with seasonal cycle), (b) R^2 of SSTa (unitless), (c) MAPE, and (d) RMSE. Note that the seasonal cycle becomes less accurate with increased forecast horizons due to increasing temperature.

During the overlapping period, the SSHA is a minimum of −2.65 for CMIP6 and −2.26 ORAS5 (Fig. 5b). The maximum SSHA is 1.02 for ORAS5 and 1.78 for CMIP6 (Fig. 5b). Like SST, most of these differences may be due to high-frequency noise (<3 month, Figs. 5a,b). However, unlike SST, the largest differences between SSHa in CMIP6 and ORAS5 are frequently greater than 1, i.e., larger than the variance (Figs. 5a,b).

As the CMIP6 ensemble mean is composed of free-running models (forced by observed changes in greenhouse gas and aerosols), it is impressive how well the sea surface temperature aligns with ORAS5 sea surface temperature (after these datasets are deseasonalized, normalized, and smoothed). Even when the CMIP6 model SST disagrees with reanalysis (e.g., during the rapid warming between 2004 and 2007, Fig. 5a), the CMIP6 models still resolve physics relevant to future ocean states. It is also surprising how well CMIP6 and ORAS5 align, considering some of the CMIP6 models have coarse (1°) resolution that may not resolve the Atlantis II Seamounts or Gulf Stream meanders (but most likely can resolve longitudinal movement). Overall, the similarity of these two datasets suggests that the CMIP6 model is suitable for training a deep learning model to predict SST at this location.

4. CNN model SST predictions

a. *Total performance*

The correlation R^2 between CNN model prediction (SST_{CNN}, where p is the prediction lead time in months) and reanalysis data (SST_{ORAS5}) is 0.99 ($p < 10^{-5}$) for all forecasts horizons and the seasonal cycle (Fig. 6a). In normalized SST anomalies, R^2 is only greater than 0.15 for forecast horizons 9–4 and 21–23 ($p < 10^{-2}$, with maximum correlations occurring at month 11 (Fig. 6b). All correlations with SST are large as the seasonal cycle captures most of the variance (Figs. 7b,d,f).

The MAPE of SST_{CNN} is less than 1.2% for all forecast horizons, with minimum error (<0.3%) occurring between 9- and 13-month predictions (Fig. 6c). In contrast, the MAPE of the seasonal cycle ranges from <1.4% (1 month) to <1.7% (Fig. 6c) so that SST_{CNN} is more accurate than the seasonal cycle for all forecast horizons. The SST_{CNN} for all months capture >44% of 1.9 Z_{SST} increases between 2013 and 2020 (Figs. 7a,c,e and 8a–c). Nine- to fourteen-month predictions resolve the seasonal (<1 yr) variability from 2000 to 2010 (Figs. 8a–c), which may contribute to the lower error relative to other forecast horizons (Fig. 6c).

RMSE varies from 0.48°C for 10-month predictions to 0.53°C for 17-month predictions (Fig. 6d). In contrast, the seasonal cycle varies from 0.68°C for 1-month prediction to 0.84°C for 24-month predictions (Fig. 6d). Unlike MAPE, the RMSE increases over the time series (Figs. 6c,d). Outliers with larger errors contribute more to RMSE than MAPE [Eqs. (3) and (4)], and as 24-month predictions have more outliers in the period from 2016 to 2018 (Figs. 8a–c), we expect RMS to increase for longer forecast horizons.

While our model predictions are superior to the 1958–2007 seasonal cycle (SST_{full}), a seasonal cycle created from later data may better reflect increasing temperatures and make more accurate predictions. The seasonal cycle from 1980 to 1999 (the 20 preceding years to the testing period, $SST_{80–99}$) varies in MAPE from 0.82% (for 1-month prediction) to 1.14% (24-month prediction). The $SST_{80–99}$ is comparable to or better than the model predictions, even beating the model for 1–7-month forecasts (Fig. 6c). However, in RMSE, $SST_{80–99}$ ranges 0.45°–0.65°C and is less accurate than the CNN model (Fig. 6d). If we compare the previous 10 years before the testing period (i.e., a seasonal cycle from 1990 to 1999, $SST_{90–99}$), MAPE ranges from 1.41% for 24-month forecasts to 1.46% for 18-month forecasts, which is of comparable accuracy to SST_{full} (Fig. 6c). The RMSE for $SST_{90–99}$ is minimum for 1 month (0.42°C) and maximum for 18 months (0.53°C)

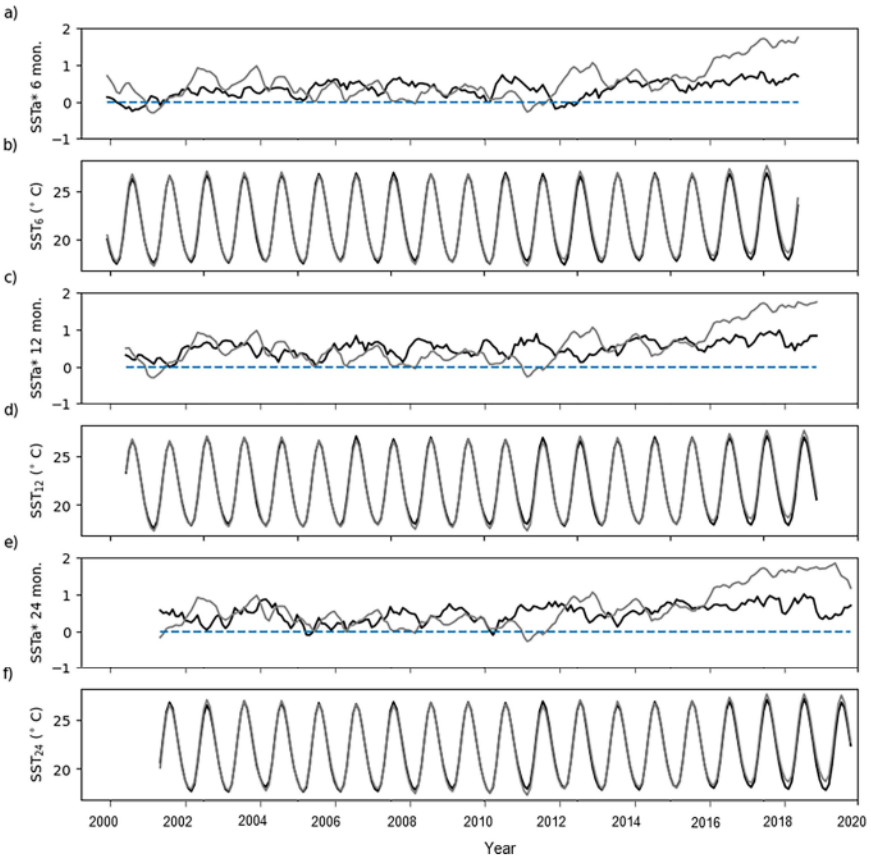


FIG. 7. Time series of SST deep learning predictions at the Atlantis II Seamounts (SST_{CNN}; black) vs ORAS5 Reanalysis (gray) for (a),(c),(e) deseasonalized normalized anomalies and (b),(d),(f) true SST for (a),(b) 6-, (c),(d) 12-, and (e),(f) 24-month forecast horizons. Blue dashed lines indicate zero (i.e., seasonal cycle, SST_{full}) on anomaly plots, which is the goal for the CNN model predictions to surpass.

and performs better as a forecast than SST_{CNN} for months 0–5 (Fig. 6d).

While $SST_{80–99}$ and $SST_{80–99}$ are more accurate than SST_{full}, they behave differently in MAPE and RMSE (Figs. 6c,d). The 1980–99 seasonal cycle (on average 0.36°C warmer than the 1958–2007 period) fits the "cool" SST regime from 2000 to 2011 (which is cooler than the preceding decade, Fig. 5a) but does poorly in the "warm" SST regime, from 2012 to 2020 (Figs. 8a–c). In contrast, the 1990–99 time period is 0.57°C warmer than the full seasonal cycle and better resolves the warm SST regime than anything other than the model prediction (Figs. 8a–c). Larger errors during the warm SST regime contribute more to RMSE despite the cool regime being a larger fraction of the testing data. The CNN model prediction for 12 and 24 months performs as well or better than each seasonal cycle for both regimes, suggesting it reflects this decadal variability.

While SST_{CNN} increases during the 2013–20 warm period [which aligns with the unprecedented shift in the Gulf Stream observed by Gonçalves Neto et al. (2021)], no values exceed SSTa equal to 1.1 (Figs. 7a,c,e), the most considerable observed value in the predictand training datasets (Fig. 5a). While limited by training data, the deep learning model still successfully predicts differences in decadal Gulf Stream regime periods. Predictions for all months do not accurately resolve the transition period in between these regimes (2010–12), with errors in SSTa approaching one standard deviation (Figs. 7a,c,e). Predictions based on the seasonal cycle calculated for a more recent warm period do not capture these regime shifts.

b. *Seasonal performance*

Over the calendar year, the greatest errors in MAPE occur in January–March (>1.32%) for forecasts greater than 12 months (Fig. 9a). The most minor errors in MAPE (>0.65%) occur from July to October, for 9–14-month predictions (Fig. 9a), and contribute to these forecast horizons having the lowest error over the testing data (Fig. 6b). However, the seasonal variability of the denominator SST_{CNN} in Eq. (4) may explain much of this seasonal distribution in MAPE, which will be larger in the summer/fall and make percent errors smaller.

However, when using RSME, errors are minimized (<2.5°C) during summer and fall months, particularly for the forecast horizons of 6–15 months (Fig. 9b). Unlike MAPE, RMSE is highest (>3.5°C) in May–July for 14–16-month predictions

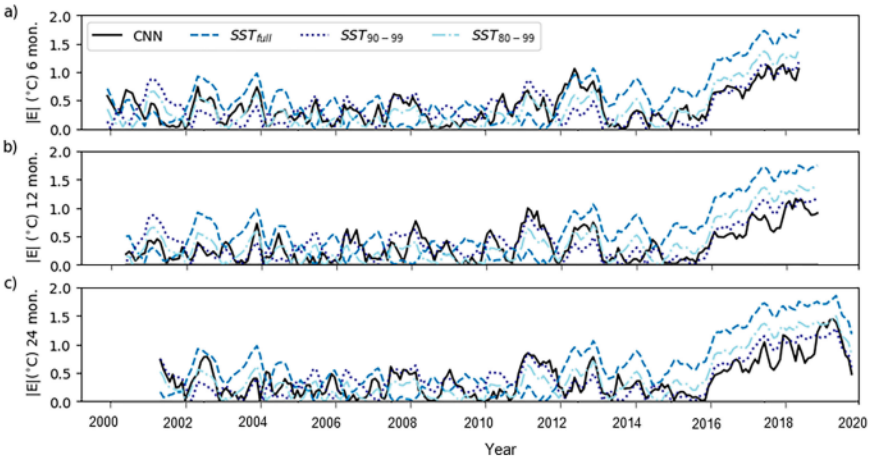


FIG. 8. Time series of SST absolute error for predictions at the Atlantis II Seamounts for the CNN model (SST_{CNN}; black), 1958–2007 seasonal cycle (SST_{full}; medium blue dash), the 1980–99 seasonal cycle ($SST_{80–99}$; light blue broken), and the 1990–99 seasonal cycle ($SST_{80–99}$; dark blue dot), from ORAS5 reanalysis for (a) 6-, (b) 12-, and (c) 24-month forecast horizons. While the CNN model consistently beats the full seasonal cycle, carefully choosing decades to calculate the seasonal cycle yields comparable results to the model but during different decadal regimes.

(Fig. 9b). The model is most successful at the 9–14-month predictions due to its ability to resolve the SST in the Atlantis II Seamounts during the seasonal temperature maxima in the fall but is weakest from April to June, which suggests difficulty in predicting variability in the timing of this warming (Fig. 7d).

Diagonal "stripes" are visible in both MAPE and RMSE (Figs. 9a,b), suggesting that the start month for predictions may be more important than the forecast horizon. For example, the period of minimum RMSE error from August to October (9–13-month forecast horizon) is only less than 2.2°C for predictions made in December–February (Figs. 9a,b). Note that the sample size is 19 for each calculation of monthly error, and outlier forecasts may affect the error, particularly in RMSE. One possible explanation is that the North Atlantic Oscillation is more predictable when forecasts are made from December to February relative to other months (Tian and Fan 2019). Another is that mixed layer depth persistence and reemergence during wintertime mixing may impact SST anomalies in the Gulf Stream and increase predictability from winter months (de Coëtlogon and Frankignoul 2003; Deser et al. 2003).

5. Teleconnections to the Atlantis II seamounts

As the CNN model can capture decadal variability at the Atlantis II Seamounts, we use backward relevancy propagation to explore how the neural network behaves in the first input month for SST, SSHAs, and MLD. In January 2010 (during the cool SST regime), saliency for SST is elevated (>0.35) in the eastern tropical Pacific, along 30°–40°N in the North Atlantic, East of Greenland, and in the northern Indian Ocean (Fig. 10a). This saliency matches most warm SST anomalies found in the Northern Hemisphere (Figs. 10a,b). While less relevant than SST, SSH saliency is greatest (>0.25) in the tropical Atlantic and patches of the north and South Pacific and may resolve eddies associated with the Kuroshio and in the North Atlantic (Figs. 10c,d). MLD saliency is largest (>0.35) in the Southern Ocean near Antarctica and in the North Atlantic (Figs. 10e,f). SST has the strongest saliency for predicting SST despite SSHAs having the most variance (Figs. 10a–f).

In January 2015, SST saliency is lower (<0.33) than January 2010, and this saliency is distributed more evenly across the

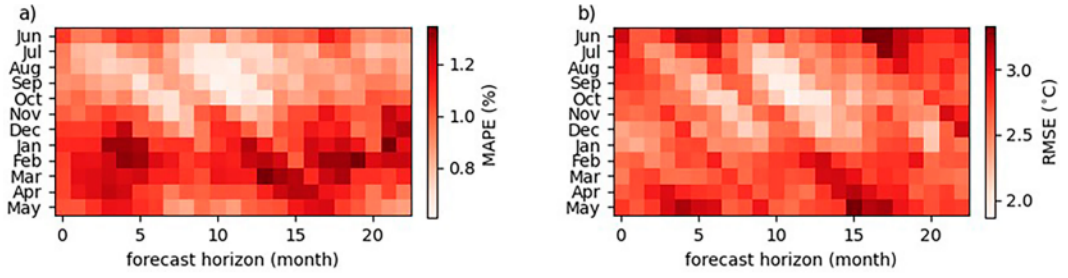


FIG. 9. Error of SST predictions over the testing dataset for each calendar month (vertical axis), for forecast horizons 1–24 months (horizontal axis) for (a) MAPE and (b) RMSE.

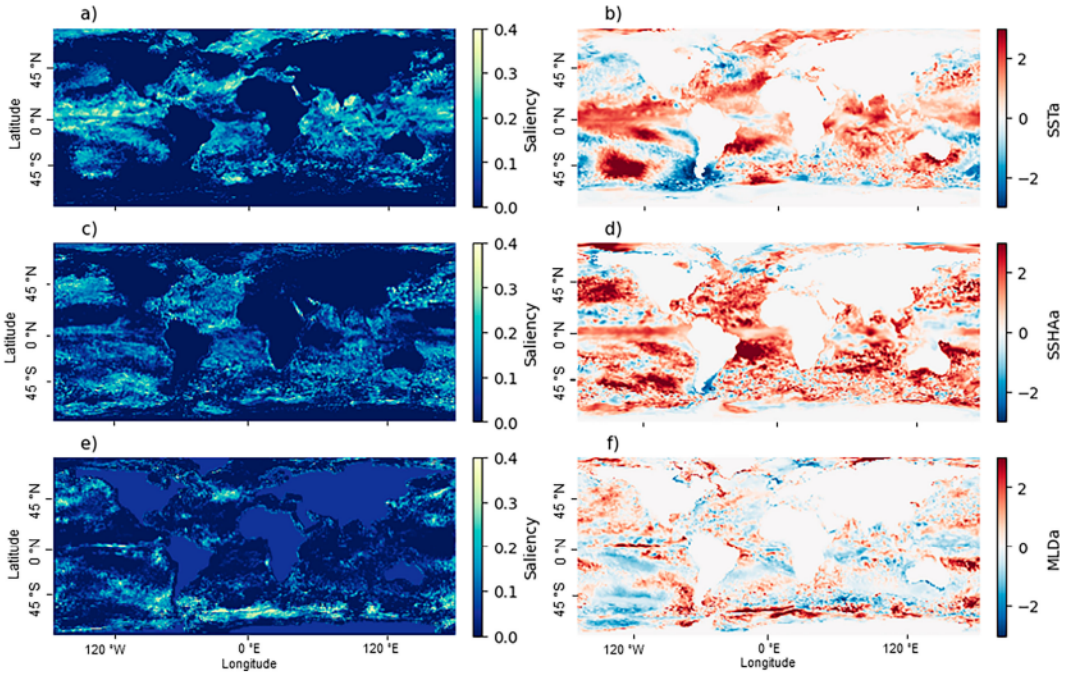


FIG. 10. Backward relevancy propagation saliency maps for (a) SST, (c) MLD, and (d) SSHAs for January 2010, a year during the cooler SST regime. (b),(d),(f) The corresponding anomaly input map is to the left of the image.

elevated temperatures of the Northern Hemisphere's oceans (Figs. 11a,b). Saliency in SSHAs (>0.25) resolves eddies in both the Atlantic and in the region of the Kuroshio (>0.25) (Figs. 11c,d). In MLD, saliency is strongest (>0.35) in the South Atlantic (Figs. 11e,f). One of the biggest differences between 2015 and 2010 is the northward shift of the Gulf Stream, which is visible in both SSTa and SSHa and captured in the SST saliency map (Figs. 11a–d). The decrease in SST

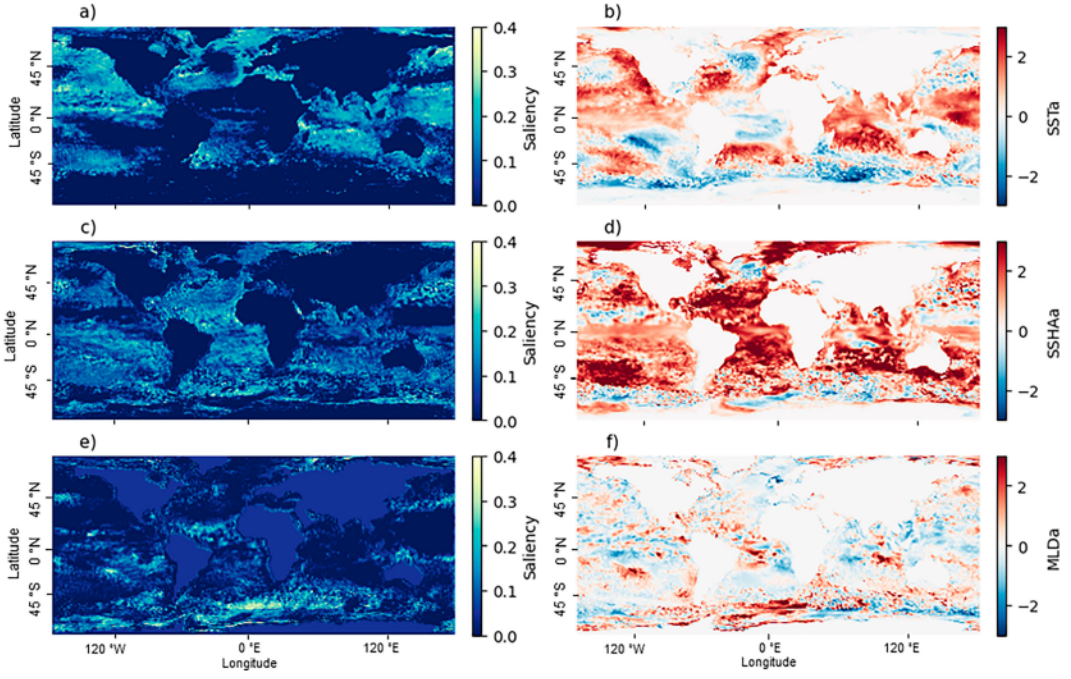


FIG. 11. Backward relevancy propagation saliency maps for (a) SST, (c) MLD, and (d) SSHAs for January 2015, a year during the warm regime. (b),(d),(f) The corresponding anomaly input map is to the left of the image. Note the northward Gulf Stream that the SST saliency map captures.

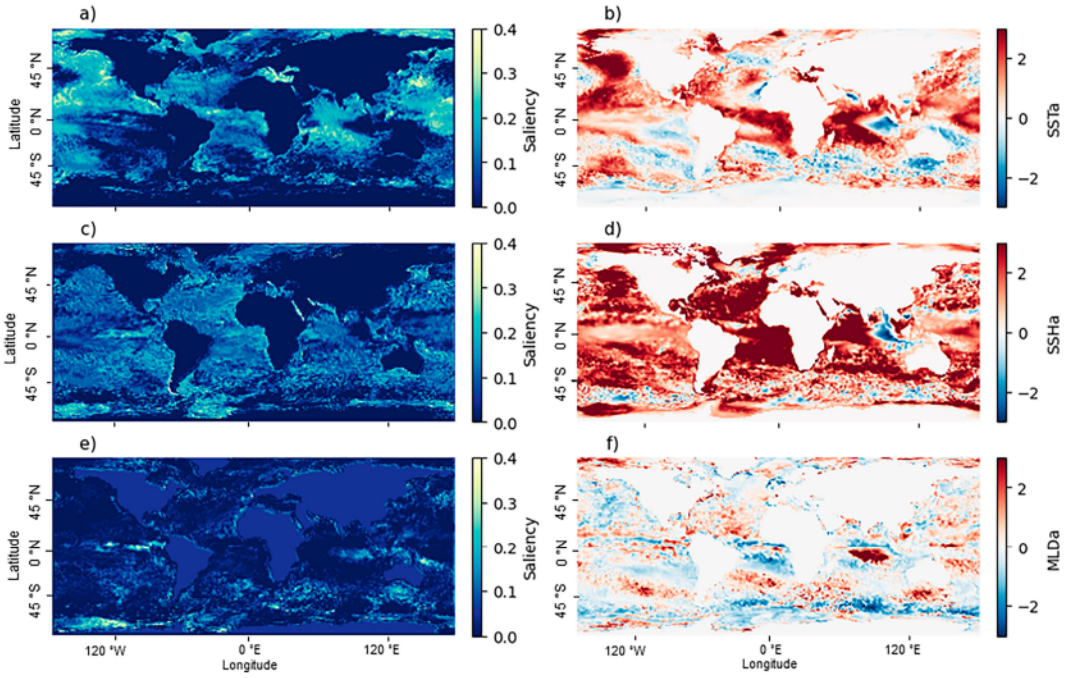


FIG. 12. Backward relevancy propagation saliency maps for (a) SST, (c) MLD, and (d) SSHAs for January 2020, a year during a positive IOD event. (b),(d),(f) The corresponding anomaly input map is to the left of the image. Note positive ENSO and the IOD event reflected in the CNN saliency map for SSTa.

saliency between 2010 and 2015 suggests that warming during 2015 may be too different from the training data to make forecasts as accurately as during 2010.

In both 2010 and 2015, the SST distribution in the North Atlantic is consistent with the SST for the positive phase of the NAO and the negative phase of the Arctic Oscillation (accounting for the lag in ocean response, Figs. 10 and 11a,b), which is positive during the months before these observations (Taylor and Gangopadhyay 2001; Paolini et al. 2024; Lim et al. 2019). The increase in MLD saliency in the North Atlantic could reflect a deepening of the MLD due to NAO-driven storms. The northern Pacific has elevated saliency during 2015 (Fig. 11), a positive year in the Pacific decadal oscillation (Johnson et al. 2020). The equatorial Pacific has elevated saliency in SST for both years, suggesting that ENSO is critical to the CNN model (Figs. 10a,b and 11a,b), but no intense ENSO event occurs during these months, although the CNN may be picking up on ENSO precursor states. Both of these years are weak negative Indian Ocean dipole events (with 2010 stronger than 2015, Liu et al. 2023), and the SST saliency highlights these SST distributions, particularly in the Bay of Bengal in 2009 (Figs. 10a,b and 11).

A weak ENSO and strong IOD positive event precedes January 2020 (Wang et al. 2023) and is visible in both SSTa and SSHa (Figs. 12b,d). The saliency map for SST captures both the Indian Ocean dipole and ENSO (Figs. 12b,d). This time period is also positive for the Pacific decadal oscillation, and the SSTa and saliency reflect this change in SST (Figs. 12a,b). As the Gulf Stream shifts northward (i.e., SST becomes warmer at Atlantis II Seamounts) after positive ENSO events modify global wind patterns (Taylor et al. 1998) and the IOD also modifies global wind patterns and is semicoupled to ENSO (Saji and Yamagata 2003), we expect the neural network to activate over these regions during these events.

6. Summary and discussion

The CMIP6 ensemble comprises of free-running models that should resolve the physics of the Gulf Stream. While not identical, the CMIP6 ensemble mean and ORAS5 have enough similarities in decadal variability to train and test a neural network model. In some cases, differences between CMIP6 and reanalysis may be advantageous in training the model. For example, the CMIP6 warms more quickly than ORAS5, and incorporating this into the training data may have helped our CNN model predictions make this increase in temperature. We should note that we tested various ensemble members, and the CMIP6 ensemble mean was the only training dataset to beat the seasonal cycle. As the ensemble mean has the most accurate SST globally, this suggests the ensemble mean is also most accurately resolving the physics relevant to the Gulf Stream position. While our current model has enough spatial resolution to resolve latitudinal shifts in position, future use of high-resolution MIPS to train CNN predictive models may more accurately resolve features such as Gulf Stream meanders. To improve this model, efforts could incorporate atmospheric data or include CMIP6 future simulations to better resolve the Gulf Stream under modern warm SST conditions so that training data might capture the same range of conditions as the testing data.

The CNN model reflects the decadal regime shift in SST from 2000–2011 to 2012–19, characterized by the northward movement of the Gulf Stream, but is limited in the warmest regime by a lack of training data in those extreme conditions. Despite this, the model predictions beat the seasonal cycle in almost all periods. Although predictions using a seasonal cycle calculated over carefully chosen time periods could produce forecasts of comparable skill to the CNN model, the substantial decadal variability may make selecting the correct period difficult. Using a trend with a seasonal cycle is also problematic, as the decadal variability is not a linear warming trend. For example, the decade 1990–99 is a worse predictor for 2000–11 due to the latter period being cooler due to the southward movement of the Gulf Stream on a decadal scale.

We tuned the model to optimize forecasts in the +7-month horizon range. However, it is still surprising how poor the 1–6-month forecasts are relative to the 9–14-month ones, suggesting that the model captures teleconnections important for longer time scales. While of less interest to this paper, models should be tuned and run separately for shorter lead time to improve accuracy. The CNN model best predicts these later months when predicted from December to February. This seasonality in prediction may be due to the imprint that deep winter mixed layers (that form during these months) have on surface temperature anomalies in the Gulf Stream despite strong lateral advection in the region. The NAO is most predictable in forecasts started during boreal winter (and the NAO is the most well-known driver of Gulf Stream variability), so the model may leverage NAO dynamics to make SST predictions. NAO SST signatures appear in backward relevancy propagation maps, along with features suggestive of the Pacific decadal oscillation (which, to our knowledge, has not been previously connected to Gulf Stream dynamics) and semicoupled ENSO and IOD in the tropical Pacific and Indian Oceans. All of these changes in SST will interact with each other through teleconnections, impact global wind patterns, and (with a lag in ocean response) modify the position of the Gulf Stream. The seasonality of the predictions also suggests separating the model to tune for forcing relevant to that season.

Our CNN model leverages these modes of global climate variability to make long-term forecasts at the Atlantis II Seamounts. These global patterns are frequently weighted more in neural network connections than local features in the Gulf Stream and North Atlantic that may impact ocean circulation for the Atlantis II Seamounts on shorter time scales. One possible way to address this would be to include coupled atmospheric variables in a semicoupled CNN.

While our current study is a simple test case, the success of this model at 1–2-yr forecasts has implications for future machine learning modeling efforts to predict ocean states at global scales. For example, different ocean areas may need to be tuned differently, such as western boundary currents (like the Gulf Stream) whose physics and interaction with wind patterns are unique to the global ocean. Isolating these patches of the ocean may also aid in the interpretation of models. Similarly, different forecast horizons may need different tuning as the dominant physical forcing mechanisms also differ. As neural network techniques rapidly evolve, our success with this simple model bodes well for more sophisticated models predicting ocean states at these forecast horizons or longer. Finally, the simplicity of our model allows us to identify climate modes of variability that contribute to SST at the Atlantis II Seamounts. Interpretable CNN models have the potential to recognize contributions of forcing in nonlinear systems beyond correlations and linear regression.

Acknowledgments. We gratefully acknowledge the support of the Chief of Naval Research through the NRL Base Program, 6.1 Scales of Ocean Atmosphere Interactive Processes, and Interactive Relationships between Atmospheric Convection and Subseasonal Oceanic Modes along the equator (PE 61153N).

Data availability statement. The data used in this paper include the European Centre for Medium-Range Weather Forecasts' Ocean Reanalysis System 5 (ORAS5) and its real-time analysis component SST, SSH, and MLD, obtained from Copernicus Climate Change Service (cds.climate.copernicus.eu). We obtained CMIP6 data in this paper at https://storage.googleapis.com/cmip6/pangeo-cmip6.json, and models and institutions are in Table 1.

TABLE 1. CMIP6 model members and institution used to make CMIP6 ensemble mean; all members are ocean monthly resolution historical runs.

Institution	Model
NCAR	CESM2-FV2
NUIST	NESM3
THU	CIESM
CCCma	CanESM5
NASA-GISS	GISS-E2-1-G
MRI	MRI-ESM2-0
IPSL	IPSL-CM6A-LR
NCC	NorESM2-LM
MPI-M	MPI-ESM1-2-LR
NCAR	CESM2
CAS	FGOALS-g3
CAMS	CAMS-CSM1-0
HAMMOZ-Consortium	MPI-ESM-1-2-HAM
CAS	FGOALS-f3-L
EC-Earth-Consortium	EC-Earth3-Veg
BCC	BCC-ESM1
NASA-GISS	GISS-E2-1-H
EC-Earth-Consortium	EC-Earth3-Veg-LR
NOAA-GFDL	GFDL-ESM4
CSIRO-ARCCSS	ACCESS-CM2
FIO-QLNM	FIO-ESM-2-0
NCAR	CESM2-WACCM
NCC	NorESM2-MM
MIROC	MIROC6
BCC	BCC-CSM2-MR

REFERENCES

Airlangga, G., 2024: Forecasting climate change impacts using machine learning and deep learning: A comparative analysis. *J-SAKTI*, **8**, 255–262, https://doi.org/10.30645/j-sakti.v8i1.784.

Ali, A., A. Fathalla, A. Salah, M. Bekhit, and E. Eldesouky, 2021: Marine data prediction: An evaluation of machine learning, deep learning, and statistical predictive models. *Comput. Intell. Neurosci.*, **2021**, 8551167, https://doi.org/10.1155/2021/8551167.

Ardabili, S., A. Mosavi, M. Dehghani, and A. R. Várkonyi-Kóczy, 2019: Deep learning and machine learning in hydrological processes climate change and Earth systems a systematic review. *Engineering for Sustainable Future*, Springer, 52–62.

Bachelery, M.-L., J. Brajard, M. Patacchiola, S. Illig, and N. Keenlyside, 2024: Predicting Atlantic and Benguela Niño events with deep learning. *Sci. Adv.*, **11**, eads5185, https://doi.org/10.1126/sciadv.ads5185.

Bader, J., and M. Latif, 2005: North Atlantic Oscillation response to anomalous Indian Ocean SST in a coupled GCM. *J. Climate*, **18**, 5382–5389, https://doi.org/10.1175/JCLI3577.1.

Bane, J. M., Jr., and W. K. Dewar, 1988: Gulf Stream bimodality and variability downstream of the Charleston bump. *J. Geophys. Res.*, **93**, 6695–6710, https://doi.org/10.1029/JC093iC06p06695.

Barnes, A. P., N. McCullen, and T. R. Kjeldsen, 2023: Forecasting seasonal to sub-seasonal rainfall in Great Britain using convolutional-neural networks. *Theor. Appl. Climatol.*, **151**, 421–432, https://doi.org/10.1007/s00704-022-04242-x.

Barnston, A. G., and R. E. Livezey, 1987: Classification, seasonality and persistence of low-frequency atmospheric circulation patterns. *Mon. Wea. Rev.*, **115**, 1083–1126, https://doi.org/10.1175/1520-0493(1987)115<1083:CSAPOL>2.0.CO;2.

Bellenger, H., E. Guilyardi, J. Leloup, M. Lengaigne, and J. Vialard, 2014: ENSO representation in climate models: From CMIP3 to CMIP5. *Climate Dyn.*, **42**, 1999–2018, https://doi.org/10.1007/s00382-013-1783-z.

Bjerknes, J., 1969: Atmospheric teleconnections from the equatorial Pacific. *Mon. Wea. Rev.*, **97**, 163–172, https://doi.org/10.1175/1520-0493(1969)097<0163:ATFTEP>2.3.CO;2.

Bommer, P. L., M. Kretschmer, A. Hedström, D. Bareeva, and M. M.-C. Höhne, 2024: Finding the right XAI method—A guide for the evaluation and ranking of explainable AI methods in climate science. *Artif. Intell. Earth Syst.*, **3**, e230074, https://doi.org/10.1175/AIES-D-23-0074.1.

Borchert, L. F., M. B. Menary, D. Swingedouw, G. Sgubin, L. Hermanson, and J. Mignot, 2021: Improved decadal predictions of North Atlantic subpolar gyre SST in CMIP6. *Geophys. Res. Lett.*, **48**, e2020GL091307, https://doi.org/10.1029/2020GL091307.

Caesar, L., S. Rahmstorf, A. Robinson, G. Feulner, and V. Saba, 2018: Observed fingerprint of a weakening Atlantic Ocean overturning circulation. *Nature*, **556**, 191–196, https://doi.org/10.1038/s41586-018-0006-5.

Carnes, M. R., 2009: Description and evaluation of GDEM-V 3.0. Naval Research Laboratory Rep. NRL/MR/7330-09-9165, 27 pp.

Chaudhuri, A. H., A. Gangopadhyay, and J. J. Bisagni, 2011: Response of the Gulf Stream transport to characteristic high and low phases of the North Atlantic Oscillation. *Ocean Modell.*, **39**, 220–232, https://doi.org/10.1016/j.ocemod.2011.04.005.

Chen, J., and Coauthors, 2023: Reduced deep convection and bottom water formation due to Antarctic meltwater in a multimodel ensemble. *Geophys. Res. Lett.*, **50**, e2023GL106492, https://doi.org/10.1029/2023GL106492.

Cheng, L., and J. Zhu, 2016: Benefits of CMIP5 multimodel ensemble in reconstructing historical ocean subsurface temperature variations. *J. Climate*, **29**, 5393–5416, https://doi.org/10.1175/JCLI-D-15-0730.1.

Chi, L., C. L. Wolfe, and S. Hameed, 2021: Has the Gulf Stream slowed or shifted in the altimetry era? *Geophys. Res. Lett.*, **48**, e2021GL093113, https://doi.org/10.1029/2021GL093113.

Choi, H.-M., M.-K. Kim, and H. Yang, 2023: Deep-learning model for sea surface temperature prediction near the Korean Peninsula. *Deep-Sea Res. II*, **208**, 105 262–105 262, https://doi.org/10.1016/j.dsr2.2023.105263.

Cullen, K., E. Shroyer, and L. O'Neill, 2022: Weakly nonlinear Ekman pumping in the Sri Lanka Dome and Southwest Monsoon Current. *J. Phys. Oceanogr.*, **52**, 1693–1703, https://doi.org/10.1175/JPO-D-21-0055.1.

de Coëtlogon, G., and C. Frankignoul, 2003: The persistence of winter sea surface temperature in the North Atlantic. *J. Climate*, **16**, 1364–1377, https://doi.org/10.1175/1520-0442-16.9.1364.

Deser, C., M. A. Alexander, and M. S. Timlin, 2003: Understanding the persistence of sea surface temperature anomalies in midlatitudes. *J. Climate*, **16**, 57–72, https://doi.org/10.1175/1520-0442(2003)016<0057:UTPOSS>2.0.CO;2.

Dong, S., M. O. Baringer, and G. J. Goni, 2019: Slow down of the Gulf Stream during 1993–2016. *Sci. Rep.*, **9**, 6672, https://doi.org/10.1038/s41598-019-42820-8.

Dorrington, J., K. Strommen, and F. Fabiano, 2021: How well does CMIP6 capture the dynamics of Euro-Atlantic weather regimes, and why? *Wea. Climate Dyn. Discuss.*, **2021**, 1–41.

Famooss Paolini, L., N.-E. Omrani, A. Bellucci, P. J. Athanasiadis, P. Ruggieri, C. R. Patrizio, and N. Keenlyside, 2024: Nonstationarity in the NAO–Gulf Stream SST front interaction. *J. Climate*, **37**, 1629–1650, https://doi.org/10.1175/JCLI-D-23-0476.1.

Feng, M., and Coauthors, 2022: Predictability of sea surface temperature anomalies at the eastern pole of the Indian Ocean Dipole—Using a convolutional neural network model. *Front. Climate*, **4**, 925068, https://doi.org/10.3389/fclim.2022.925068.

Frankignoul, C., G. de Coëtlogon, T. M. Joyce, and S. Dong, 2001: Gulf Stream variability and ocean–atmosphere interactions. *J. Phys. Oceanogr.*, **31**, 3516–3529, https://doi.org/10.1175/1520-0485(2002)031<3516:GSVAOA>2.0.CO;2.

Gangopadhyay, A., A. H. Chaudhuri, and A. H. Taylor, 2016: On the nature of temporal variability of the Gulf Stream path from 75° to 55°W. *Earth Interact.*, **20**, https://doi.org/10.1175/EI-D-15-0025.1.

Gao, C., L. Zhou, and R.-H. Zhang, 2023: A transformer-based deep learning model for successful predictions of the 2021 second-year La Niña condition. *Geophys. Res. Lett.*, **50**, e2023GL104034, https://doi.org/10.1029/2023GL104034.

Geng, H., and T. Wang, 2021: Spatiotemporal model based on deep learning for ENSO forecasts. *Atmosphere*, **12**, 810, https://doi.org/10.3390/atmos12070810.

Gispen, D., and M. J. Schmeits, 2001: Bimodality and internal variability of the Gulf Stream and the Kuroshio. Ph.D. thesis, Utrecht University, 141 pp., https://core.ac.uk/download/pdf/39700087.pdf.

Glorot, X., A. Bordes, and Y. Bengio, 2011: Deep sparse rectifier neural networks. *Proc. 14th Int. Conf. Artificial Intelligence and Statistics*, Fort Lauderdale, FL, PMLR, 315–323, https://proceedings.mlr.press/v15/glorot11a.html.

Gonçalves Neto, A., J. A. Langan, and J. B. Palter, 2021: Changes in the Gulf Stream preceded rapid warming of the Northwest

Atlantic Shelf. *Commun. Earth Environ.*, **2**, 74, https://doi.org/10.1038/s43247-021-00143-5.

Guo, Y., S. Bishop, F. Bryan, and S. Bachman, 2023: Mesoscale variability linked to interannual displacement of Gulf Stream. *Geophys. Res. Lett.*, **50**, e2022GL102549, https://doi.org/10.1029/2022GL102549.

Ham, Y.-G., J.-H. Kim, and J.-J. Luo, 2019: Deep learning for multi-year ENSO forecasts. *Nature*, **573**, 568–572, https://doi.org/10.1038/s41586-019-1559-7.

Hamdan, A., K. I. Ibekwe, E. A. Etukudoh, A. A. Umoh, and V. I. Ilojianya, 2024: AI and machine learning in climate change research: A review of predictive models and environmental impact. *World J. Adv. Res. Rev.*, **21**, 1999–2008, https://doi.org/10.30574/wjarr.2024.21.1.0257.

Hameed, S., C. L. Wolfe, and L. Chi, 2018: Impact of the Atlantic meridional mode on Gulf Stream North Wall position. *J. Climate*, **31**, 8875–8894, https://doi.org/10.1175/JCLI-D-18-0098.1.

Hamid, K., W. Collins, P. Tissot, S. A. King, H. T. H. Dinh, N. Durham, and J. Rizzo, 2021: FogNet: A multiscale 3D CNN with double-branch dense block and attention mechanism for fog prediction. *Mach. Learn. Appl.*, **5**, 100038, https://doi.org/10.1016/j.mlwa.2021.100038.

Hand, R., N. S. Keenlyside, N.-E. Omrani, J. Bader, and R. J. Greatbatch, 2019: The role of local sea surface temperature pattern changes in shaping climate change in the North Atlantic sector. *Climate Dyn.*, **52**, 417–438, https://doi.org/10.1007/s00382-018-4151-1.

He, D., P. Lin, H. Liu, L. Ding, and J. Jiang, 2019: DLENSO: A deep learning ENSO forecasting model. *PRICAI 2019: Trends in Artificial Intelligence: 16th Pacific Rim Int. Conf. on Artificial Intelligence, Cuvu, Yanuca Island, Fiji, Proc., Part II 16*, Cham, Springer, 12–23, https://doi.org/10.1007/978-3-030-29911-8_2.

Hu, A., and S. C. Bates, 2018: Internal climate variability and projected future regional steric and dynamic sea level rise. *Nat. Commun.*, **9**, 1068, https://doi.org/10.1038/s41467-018-03474-8.

Janmaijaya, M., M. Janmaijaya, and P. K. Muhuri, 2024: A novel model based on spatio-temporal dilated ConvLSTM networks for Indian Ocean dipole forecasting using multi-source global sea surface temperature and heat content data. *IEEE Access*, **12**, 75 781–75 791, https://doi.org/10.1109/ACCESS.2024.3376520.

Jeon, S., and J. Kim, 2024: Artificial intelligence to predict climate and weather change. *JMST Adv.*, **6**, 67–73, https://doi.org/10.1007/s42791-024-00068-y.

Jiménez-Esteve, B., and D. I. Domeisen, 2020: Nonlinearity in the tropospheric pathway of ENSO to the North Atlantic. *Wea. Climate Dyn.*, **1**, 225–245, https://doi.org/10.5194/wcd-1-225-2020.

Johnson, Z. F., Y. Chikamoto, S.-Y. S. Wang, M. J. McPhaden, and T. Mochizuki, 2020: Pacific decadal oscillation remotely forced by the equatorial Pacific and the Atlantic Oceans. *Climate Dyn.*, **55**, 789–811, https://doi.org/10.1007/s00382-020-05295-2.

Joyce, T. M., and R. Zhang, 2010: On the path of the Gulf Stream and the Atlantic meridional overturning circulation. *J. Climate*, **23**, 3146–3154, https://doi.org/10.1175/2010JCLI3310.1.

——, Y.-O. Kwon, and L. Yu, 2009: On the relationship between synoptic wintertime atmospheric variability and path shifts in the Gulf Stream and the Kuroshio extension. *J. Climate*, **22**, 3177–3192, https://doi.org/10.1175/2008JCLI2690.1.

Kim, J., T. Kim, J.-G. Ryu, and J. Kim, 2023: Spatiotemporal graph neural network for multivariate multi-step ahead time-series forecasting of sea temperature. *Eng. Appl. Artif. Intell.*, **126**, 106854, https://doi.org/10.1016/j.engappai.2023.106854.

Kohyama, T., Y. Yamagami, H. Miura, S. Kido, H. Tatebe, and M. Watanabe, 2021: The Gulf Stream and Kuroshio Current are synchronized. *Science*, **374**, 341–346, https://doi.org/10.1126/science.abh3295.

Krestenitis, M., Y. Androulidakis, and Y. Krestenitis, 2024: Deep learning-based forecasting of sea surface temperature in the interim future: Application over the Aegean, Ionian, and Cretan Seas (NE Mediterranean Sea). *Ocean Dyn.*, **74**, 149–168, https://doi.org/10.1007/s10236-023-01595-3.

Lam, R., and Coauthors, 2022: GraphCast: Learning skillful medium-range global weather forecasting. arXiv, 2212.12794v2, https://doi.org/10.48550/arXiv.2212.12794.

Lim, Y.-K., R. I. Cullather, S. M. Nowicki, and K.-M. Kim, 2019: Inter-relationship between subtropical Pacific sea surface temperature, Arctic sea ice concentration, and North Atlantic Oscillation in recent summers. *Sci. Rep.*, **9**, 3481, https://doi.org/10.1038/s41598-019-39896-7.

Ling, F., J.-J. Luo, Y. Li, T. Tang, L. Bai, W. Ouyang, and T. Yamagata, 2022: Multi-task machine learning improves multi-seasonal prediction of the Indian Ocean dipole. *Nat. Commun.*, **13**, 7681, https://doi.org/10.1038/s41467-022-35412-0.

Liu, A., J. Zuo, B. Tian, and B. Lu, 2023: Impact of Indian Ocean dipole on Atlantic Niño predictive skill. *Environ. Res. Lett.*, **18**, 074015, https://doi.org/10.1088/1748-9326/acdc3c.

Liu, G., P. Wang, M. Beveridge, Y.-O. Kwon, and I. Drori, 2021: Predicting Atlantic multidecadal variability. arXiv, 2111.00124v1, https://doi.org/10.48550/arXiv.2111.00124.

Liu, J., Y. Tang, Y. Wu, T. Li, Q. Wang, and D. Chen, 2021: Forecasting the Indian Ocean dipole with deep learning techniques. *Geophys. Res. Lett.*, **48**, e2021GL094407, https://doi.org/10.1029/2021GL094407.

Liu, Y., L. Zhang, W. Hao, L. Zhang, and L. Huang, 2024: Predicting temporal and spatial 4-D ocean temperature using satellite data based on a novel deep learning model. *Ocean Modell.*, **188**, 102333, https://doi.org/10.1016/j.ocemod.2024.102333.

Lops, Y., Y. Choi, S. Mousavinezhad, A. K. Salman, D. L. Nelson, and D. Singh, 2023: Development of deep convolutional neural network ensemble models for 36-month ENSO forecasts. *Asia-Pac. J. Atmos. Sci.*, **59**, 597–605, https://doi.org/10.1007/s13143-023-00319-3.

Lu, F., and Coauthors, 2020: GFDL's SPEAR seasonal prediction system: Initialization and ocean tendency adjustment (OTA) for coupled model predictions. *J. Adv. Model. Earth Syst.*, **12**, e2020MS002149, https://doi.org/10.1029/2020MS002149.

Luo, X., S. Yuan, B. Mu, and J. Li, 2021: The ELM model with residual compensation based on ARIMA for North Atlantic Oscillation index prediction. *IVSP'21: Proc. 2021 Third Int. Conf. on Image, Video and Signal Processing*, Singapore, Singapore, Association for Computing Machinery, 122–126, https://doi.org/10.1145/3459212.3459231.

Mamalakis, A., E. A. Barnes, and I. Ebert-Uphoff, 2022: Investigating the fidelity of explainable artificial intelligence methods for applications of convolutional neural networks in geoscience. *Artif. Intell. Earth Syst.*, **1**, e220012, https://doi.org/10.1175/AIES-D-22-0012.1.

McCarthy, G., and Coauthors, 2012: Observed interannual variability of the Atlantic meridional overturning circulation at 26.5°N. *Geophys. Res. Lett.*, **39**, L19609, https://doi.org/10.1029/2012GL052933.

Mu, B., J. Li, S. Yuan, and X. Luo, 2020: Prediction of North Atlantic Oscillation index associated with the sea level pressure using DWT-LSTM and DWT-ConvLSTM networks. *Math. Probl. Eng.*, **2020**, 2413041, https://doi.org/10.1155/2020/2413041.

——, B. Qin, and S. Yuan, 2021: ENSO-ASC 1.0.0: ENSO deep learning forecast model with a multivariate air–sea coupler. *Geosci. Model Dev.*, **14**, 6977–6999, https://doi.org/10.5194/gmd-14-6977-2021.

——, X. Jiang, S. Yuan, Y. Cui, and B. Qin, 2023: NAO seasonal forecast using a multivariate air–sea coupled deep learning model combined with causal discovery. *Atmosphere*, **14**, 792, https://doi.org/10.3390/atmos14050792.

Nigam, S., A. Ruiz-Barradas, and L. Chafik, 2018: Gulf Stream excursions and sectional detachments generate the decadal pulses in the Atlantic multidecadal oscillation. *J. Climate*, **31**, 2853–2870, https://doi.org/10.1175/JCLI-D-17-0010.1.

Pan, B., G. J. Anderson, A. Goncalves, D. D. Lucas, C. J. Bonfils, and J. Lee, 2022: Improving seasonal forecast using probabilistic deep learning. *J. Adv. Model. Earth Syst.*, **14**, e2021MS002766, https://doi.org/10.1029/2021MS002766.

Pratt, L., J. Earles, P. Cornillon, and J.-F. Cayula, 1991: The nonlinear behavior of varicose disturbances in a simple model of the Gulf Stream. *Deep-Sea Res.*, **38A** (Supplement 1), S591–S622, https://doi.org/10.1016/S0198-0149(12)80025-2.

Qi, J., T. Qu, and B. Yin, 2023: Meta-learning-based estimation of the barrier layer thickness in the tropical Indian Ocean. *Environ. Res. Commun.*, **5**, 091005, https://doi.org/10.1088/2515-7620/acf9e1.

Ratnam, J., H. Dijkstra, and S. K. Behera, 2020: A machine learning based prediction system for the Indian Ocean dipole. *Sci. Rep.*, **10**, 284, https://doi.org/10.1038/s41598-019-57162-8.

Rebuffi, S.-A., R. Fong, X. Ji, and A. Vedaldi, 2020: There and back again: Revisiting backpropagation saliency methods. *Proc. IEEE/CVF Conf. on Computer Vision and Pattern Recognition*, Seattle, WA, Institute of Electrical and Electronics Engineers, 8839–8848, https://doi.org/10.1109/CVPR42600.2020.00886.

Richter, I., and H. Tokinaga, 2020: An overview of the performance of CMIP6 models in the tropical Atlantic: Mean state, variability, and remote impacts. *Climate Dyn.*, **55**, 2579–2601, https://doi.org/10.1007/s00382-020-05409-w.

Rivera Tello, G. A., K. Takahashi, and C. Karamperidou, 2023: Explained predictions of strong eastern Pacific El Niño events using deep learning. *Sci. Rep.*, **13**, 21150, https://doi.org/10.1038/s41598-023-45739-3.

Saba, V. S., and Coauthors, 2016: Enhanced warming of the Northwest Atlantic Ocean under climate change. *J. Geophys. Res. Oceans*, **121**, 118–132, https://doi.org/10.1002/2015JC011346.

Saji, N., and T. Yamagata, 2003: Possible impacts of Indian Ocean Dipole mode events on global climate. *Climate Res.*, **25**, 151–169, https://doi.org/10.3354/cr025151.

Sanchez-Franks, A., and R. Zhang, 2015: Impact of the Atlantic meridional overturning circulation on the decadal variability of the Gulf Stream path and regional chlorophyll and nutrient concentrations. *Geophys. Res. Lett.*, **42**, 9889–9887, https://doi.org/10.1002/2015GL066262.

——, S. Hameed, and R. E. Wilson, 2016: The Icelandic low as a predictor of the Gulf Stream north wall position. *J. Phys. Oceanogr.*, **46**, 817–826, https://doi.org/10.1175/JPO-D-14-0244.1.

Sardana, D., P. Kumar, and Rajni, 2024: CMIP6 model evaluation for sea surface height responses to ENSO. *Climate Dyn.*, **62**, 1829–1847, https://doi.org/10.1007/s00382-023-06997-z.

Sarkar, P. P., P. Janardhan, and P. Roy, 2020: Prediction of sea surface temperatures using deep learning neural networks. *SN Appl. Sci.*, **2**, 1458, https://doi.org/10.1007/s42452-020-03239-3.

——, ——, and ——, 2021: A novel deep neural network model approach to predict Indian Ocean dipole and Equatorial Indian Ocean oscillation indices. *Dyn. Atmos. Oceans*, **96**, 101266, https://doi.org/10.1016/j.dynatmoce.2021.101266.

Sato, O. T., and T. Rossby, 1995: Seasonal and low frequency variations in dynamic height anomaly and transport of the Gulf Stream. *Deep-Sea Res. I*, **42**, 149–164, https://doi.org/10.1016/0967-0637(94)00034-P.

Scafetta, N., 2023: CMIP6 GCM ensemble members versus global surface temperatures. *Climate Dyn.*, **60**, 3091–3120, https://doi.org/10.1007/s00382-022-06493-w.

Seidov, D., A. Mishonov, J. Reagan, and R. Parsons, 2019: Resilience of the Gulf Stream path on decadal and longer timescales. *Sci. Rep.*, **9**, 11549, https://doi.org/10.1038/s41598-019-48011-9.

Smeed, D. A., and Coauthors, 2018: The North Atlantic Ocean is in a state of reduced overturning. *Geophys. Res. Lett.*, **45**, 1527–1533, https://doi.org/10.1002/2017GL076350.

Snoussi, M., A. Tamim, S. E. Fellah, and L. Koutti, 2024: Spatio-temporal prediction of monthly coastal upwelling scenario in SST fields using deep-learning-based models. *IEEE Geosci. Remote Sens. Lett.*, **21**, 1–5, https://doi.org/10.1109/LGRS.2024.3381438.

Su, H., F. Zhang, J. Teng, A. Wang, and Z. Huang, 2024: Reconstructing high-resolution subsurface temperature of the global ocean using deep forest with combined remote sensing and in situ observations. *ISPRS J. Photogramm. Remote Sens.*, **218**, 389–404, https://doi.org/10.1016/j.isprsjprs.2024.09.022.

Tang, Y., and A. Duan, 2021: Using deep learning to predict the East Asian summer monsoon. *Environ. Res. Lett.*, **16**, 124006, https://doi.org/10.1088/1748-9326/ac34bc.

Taylor, A. H., and J. A. Stephens, 1998: The North Atlantic Oscillation and the latitude of the Gulf Stream. *Tellus*, **50A**, 134–142, https://doi.org/10.3402/tellusa.v50i1.14517.

——, and A. Gangopadhyay, 2001: A simple model of interannual displacements of the Gulf Stream. *J. Geophys. Res.*, **106**, 13 849–13 860, https://doi.org/10.1029/1999JC000147.

——, M. B. Jordan, and J. A. Stephens, 1998: Gulf Stream shifts following ENSO events. *Nature*, **393**, 638–638, https://doi.org/10.1038/31380.

Taylor, J., and M. Feng, 2022: A deep learning model for forecasting global monthly mean sea surface temperature anomalies. *Front. Climate*, **4**, 932932, https://doi.org/10.3389/fclim.2022.932932.

Tian, B., and K. Fan, 2019: Why is the North Atlantic Oscillation more predictable in December? *Atmosphere*, **10**, 477, https://doi.org/10.3390/atmos10080477.

Todd, R. E., and A. S. Ren, 2023: Warming and lateral shift of the Gulf Stream from in situ observations since 2001. *Nat. Climate Change*, **13**, 1348–1352, https://doi.org/10.1038/s41558-023-01835-w.

van Straaten, C., K. Whan, D. Coumou, B. van den Hurk, and M. Schmeits, 2023: Correcting subseasonal forecast errors with an explainable ANN to understand misrepresented sources of predictability of European summer temperatures. *Artif. Intell. Earth Syst.*, **2**, e220047, https://doi.org/10.1175/AIES-D-22-0047.1.

Vastano, A. C., and B. A. Warren, 1976: Perturbations to the Gulf Stream by Atlantis II seamount. *Deep-Sea Res. Oceanogr. Abstr.*, **23**, 681–694, https://doi.org/10.1016/S0011-7471(76)80014-9.

Visbeck, M., E. P. Chassignet, R. G. Curry, T. L. Delworth, R. R. Dickson, and G. Krahmann, 2003: *The Ocean's Response to North Atlantic Oscillation Variability*. Geophysical Monograph Series, Vol. 134, Amer. Geophys. Union, 113–146.

Walters, M. W., O. A. Godin, J. E. Joseph, and T. W. Tan, 2024: Deep-water ambient sound over the Atlantis II seamounts in the Northwest Atlantic. *J. Acoust. Soc. Amer.*, **156**, 2687–2700, https://doi.org/10.1121/10.0032360.

Wang, G.-G., H. Cheng, Y. Zhang, and H. Yu, 2023: ENSO analysis and prediction using deep learning: A review. *Neurocomputing*, **520**, 216–229, https://doi.org/10.1016/j.neucom.2022.11.078.

Wang, T., and P. Huang, 2024: Superiority of a convolutional neural network model over dynamical models in predicting central Pacific ENSO. *Adv. Atmos. Sci.*, **41**, 141–154, https://doi.org/10.1007/s00376-023-3001-1.

Watelet, S., J.-M. Beckers, and A. Barth, 2017: Reconstruction of the Gulf Stream from 1940 to the present and correlation with the North Atlantic Oscillation. *J. Phys. Oceanogr.*, **47**, 2741–2754, https://doi.org/10.1175/JPO-D-17-0064.1.

Webster, P. J., A. M. Moore, J. P. Loschnigg, and R. R. Leben, 1999: Coupled ocean-atmosphere dynamics in the Indian Ocean during 1997-98. *Nature*, **401**, 356–360, https://doi.org/10.1038/43848.

Wei, S., C. Wang, F. Zhang, and K. Yang, 2024: Prediction of seasonal sea surface temperature based on temperature and salinity of subsurface ocean using machine learning. *Int. J. Climatol.*, **44**, 1326–1338, https://doi.org/10.1002/joc.8384.

Weisheimer, A., and Coauthors, 2009: ENSEMBLES: A new multi-model ensemble for seasonal-to-annual predictions—Skill and progress beyond DEMETER in forecasting tropical Pacific SSTs. *Geophys. Res. Lett.*, **36**, L21711, https://doi.org/10.1029/2009GL040896.

Wolfe, C. L., S. Hameed, and L. Chi, 2019: On the drivers of decadal variability of the Gulf Stream north wall. *J. Climate*, **32**, 1235–1249, https://doi.org/10.1175/JCLI-D-18-0212.1.

Xiao, C., and Coauthors, 2019: A spatiotemporal deep learning model for sea surface temperature field prediction using time-series satellite data. *Environ. Modell. Software*, **120**, 104502, https://doi.org/10.1016/j.envsoft.2019.104502.

Xie, B., J. Qi, S. Yang, G. Sun, Z. Feng, B. Yin, and W. Wang, 2024: Sea surface temperature and marine heat wave predictions in the South China Sea: A 3D U-Net deep learning model integrating multi-source data. *Atmosphere*, **15**, 86, https://doi.org/10.3390/atmos15010086.

Xie, J., J. Zhang, J. Yu, and L. Xu, 2020: An adaptive scale sea surface temperature predicting method based on deep learning with attention mechanism. *IEEE Geosci. Remote Sens. Lett.*, **17**, 740–744, https://doi.org/10.1109/LGRS.2019.2931728.

Xu, T., Z. Zhou, Y. Li, C. Wang, Y. Liu, and T. Rong, 2023: Short-term prediction of global sea surface temperature using deep learning networks. *J. Mar. Sci. Eng.*, **11**, 1352, https://doi.org/10.3390/jmse11071352.

Yamagami, Y., M. Watanabe, M. Mori, and J. Ono, 2022: Barents-Kara sea-ice decline attributed to surface warming in the Gulf Stream. *Nat. Commun.*, **13**, 3767, https://doi.org/10.1038/s41467-022-31117-6.

Yang, H., G. Lohmann, W. Wei, M. Dima, M. Ionita, and J. Liu, 2016: Intensification and poleward shift of subtropical western boundary currents in a warming climate. *J. Geophys. Res. Oceans*, **121**, 4928–4945, https://doi.org/10.1002/2015JC011513.

Yu, X., S. Shi, L. Xu, Y. Liu, Q. Miao, and M. Sun, 2020: A novel method for sea surface temperature prediction based on deep learning. *Math. Probl. Eng.*, **2020**, 1–9, https://doi.org/10.1155/2020/6387173.

Yuan, S., X. Luo, B. Mu, J. Li, and G. Dai, 2019: Prediction of North Atlantic Oscillation index with convolutional LSTM based on ensemble empirical mode decomposition. *Atmosphere*, **10**, 252, https://doi.org/10.3390/atmos10050252.

Yun, J., K.-J. Ha, and S.-S. Lee, 2024: Impact of greenhouse warming on mesoscale eddy characteristics in high-resolution climate simulations. *Environ. Res. Lett.*, **19**, 014078, https://doi.org/10.1088/1748-9326/ad114b.

Zhou, L., and R.-H. Zhang, 2024: ENSO-related precursor pathways of interannual thermal anomalies identified using a transformer-based deep learning model in the tropical Pacific. *Geophys. Res. Lett.*, **51**, e2023GL107347, https://doi.org/10.1029/2023GL107347.

Copyright of Journal of Physical Oceanography is the property of American Meteorological Society and its content may not be copied or emailed to multiple sites without the copyright holder's express written permission. Additionally, content may not be used with any artificial intelligence tools or machine learning technologies. However, users may print, download, or email articles for individual use.